Synthesis of Hematite α-Fe$_2$O$_3$ Nano Powders by the controlled precipitation method

Síntesis de nano polvos de hematita α-Fe$_2$O$_3$ por el método de precipitación controlada

Jimmy Alexander Morales-Morales [a]*

Abstract

Recently increased attention has been paid to the synthesis of hematite nanoparticles, due to its properties and application in various fields of modern technology. The aqueous route has shown to be simpler and more versatile than the non-aqueous routes. In this study, nanopowder particles of α-Fe$_2$O$_3$ (hematite) were synthesized by controlled precipitation method in three stages: precursors' precipitation, washing and calcination. The precipitation was controlled with ferric chloride as precursor, and sodium hydroxide as precipitant, in constant agitation and pH 6.

There were tested with different reaction times: With 1 and 2 days. With one day reaction, the synthesis of hematite accompanied by maghemite, was verified by XRD. After 2 days of the reaction was proved that it is possible to obtain hematite and maghemite in greater quantities, but with magnetite impurities, and less chloride content, thanks to repeated washings. This is an interesting observation since impurities magnetite has not been reported in the synthesis of hematite by controlled precipitation method.

It was found that the reaction time and repeated washings used in the synthesis process, played an important role in determining the iron oxides and particle size, plus phase formation and transformation, which was confirmed at different reaction times and repeated washings by XRD analysis, FT-IR, Raman and SEM.

Samples with two days reaction, washed and calcined at 425 ºC, with a size less than 100 nm are associated with a hematite, magnetite and maghemite mixture, with almost a plate-shaped sphere morphology and the aggregates are formed by hemispherical primary particles, whose size apparently is in the nanometers' order.

Keywords: Magnetite, Maghemite, Hematite Nanoparticles, α-Fe$_2$O$_3$ Nanopowder, Raman.

a Research Group Chemistry and Biotechnology (QUIBIO), Faculty Basic Sciences, Santiago de Cali University, Colombia
* Corresponding author: jim.ale.mor@gmail.com

Resumen

Recientemente se ha prestado mayor atención a la síntesis de nanopartículas de hematita, debido a sus propiedades y aplicaciones en diversos campos de la tecnología moderna. La ruta acuosa ha mostrado ser más simple y más versátil que las rutas no acuosas. En este estudio se sintetizaron nanopolvos de α-Fe$_2$O$_3$ (hematita) por el método de precipitación controlada en tres etapas: precipitación de precursores, lavado y calcinación. La precipitación se controla con cloruro férrico como precursor, e hidróxido de sodio como agente de precipitación, en agitación constante y pH 6.

Se probaron con tiempos de reacción de 1 y 2 días. Con un día de reacción, se comprobó por DRX la síntesis de hematita, acompañada de maghemita; esta es una observación interesante, ya que las impurezas de magnetita no se han informado en la síntesis de hematita por el método de precipitación controlada; además, no se eliminaron los cloruros en un lavado. Después de 2 días de reacción se concluyó que es posible obtener hematita y maghemita, pero con impurezas de magnetita y menos contenido de cloruros, gracias a lavados repetidos.

Se encontró que el tiempo de reacción y los lavados repetidos utilizados en el proceso de síntesis jugaron un papel importante en la determinación de la transformación de los óxidos de hierro y del tamaño de la partícula y de la fase. La Formación/transformación de fases a diferente tiempo de reacción y lavados repetidos se confirmó por análisis XRD, FT-IR, SEM y Raman.

Las muestras con dos días de reacción, lavadas y calcinadas a 425 ºC, con tamaño < 100 nm, se asocian a una mezcla de hematita, magnetita y maghemita, con morfología casi de placas en forma de esfera, y los agregados están formados por partículas primarias semiesféricas cuyo tamaño, al parecer, es del orden de nanómetros.

Palabras clave: Magnetita, Maghemita, Nanopartículas de hematita, Nanopolvos de α-Fe$_2$O$_3$, Raman

1. Introduction

The hematite iron oxides forms ($\alpha-Fe_2O_3$) among others are of great importance in technological and industrial applications [1]. Hematite exhibits high resistance to corrosion, therefore, it has been extensively used in many fields which include photo-anode for photo assisted electrolysis of water. This is due to its favorable properties such as a band gap between 2.0–2.2 eV, which allows absorbing a substantial fraction of solar spectrum, chemical stability in aqueous environment, and nontoxicity. It is an active component of gas sensors, catalyst, lithium ion battery, pigments and oxidizer in thermite composition [2-6]. It is also used in magnetic fluids, also called ferrofluids, for damping in inertial motors, shock absorbers, heat transfer fluids, etc [7]. Because of its extensive applications, nano hematite has attracted much attention for its synthesis and applications.

For the current uses of the iron oxides in biotechnology, nanomedicine and environmental remediation, mainly requires that the particles may obtain certain characteristics, which can be achieved by controlling the oxide synthesis. Various techniques have been used to fabricate hematite nanomaterials of desired morphology (e.g. nanorods, nanofibres, nanowires, etc.) for various applications. Methods that have been employed for hematite synthesis, may either be a wet/based solution or a non-solution dry/ based. Wet synthesis include methods such as thermolysis/forced hydrolysis, precipitation/coprecipitation, which in the case of hematite might involve synthesis of an intermediate (A ferrihydrite or goethite or both), followed by dehydroxylation at high temperature [8], or Sol-gel synthesis, which involves dissolution of the Fe^{3+} and an organic compound to form the sol, concentrating the sol by removal of water to form the gel and subsequent thermal treatment to obtain the required product [9] or hydro/solvothermal synthesis, in which α-Fe_2O_3 is precipitated at high temperature (ranging from 160 to about 280°C) [10-14].

The dry methods could be either thermal decomposition/combustion processes (reaction occurs in the vapour phase. e.g. chemical vapour condensation, laser pyrolysis and arc discharge) or solid state chemical reaction (reactions take place in solid state e.g. mechanochemical high energy or ball milling, it involves milling of the precursors at high energy to form nanomaterials) [15]. However, these methods involve special equipment, high temperatures, and the tedious removal of impurities, which are all time-consuming and come at a high monetary cost.

The controlled precipitation process has been used for the preparation of nano or submicro powders, in a variety of metal oxides using inorganic salts as precursors [16]. The synthesis of magnetic nanoparticles with controlled size has long been of scientific and technological interest. However, uniform physical and chemical properties of magnetic nanoparticles, greatly depend upon the synthesis route and how to develop a simplistic and effective way to synthesize magnetic particles, with high dispersion and narrow size distribution, remains a challenge.

In this paper, ferric oxide nanopowders were synthesized by controlled precipitation route, using iron chloride precursor. Structural and surface morphological properties and the relationship synthesis-structure are described and discussed by RAMAN, FTIR, DRX and SEM (Scanning Electronic Microscopy) analyses

2. Methodology

All chemicals were of analytical grade and were used as received without further purification. Distilled water was used for the preparation of solutions and washing the synthesized samples. The synthesis of iron oxide nanopowders was carried out in 3 stages: Precipitation, washing and heat treatment, according to the following manner:

(1) Precipitation was performed with 250 ml of precursor solution of Fe (III) 1 M. A 6 M NaOH solution was then added, drop wise (drop rate = 1 ml min-1) to the stirring mixture at room temperature. The pH value was defined according to the experimental conditions given in reference [17] and was maintained during the synthesis. The resulting dispersion was continuously stirred at room temperature The reaction time was adjusted to 24 hours and 48 hours and the evolution of the synthesis was evaluated. The sample is taken every day of synthesis (sample M-I 24 hours and sample M-48 hours, calcined 450 ºC), and was examined grain size, through the metallographic microscope and analyzed by XRD, to determine the crystalline phases present in each sample.

(2) Removal of subproducts generated in the synthesis by consecutive washings. The resulting colloidal suspension, containing nanoparticles, was washed by repeated centrifugation at 3.800 rpm. The solid phase was separated and re-dispersion carried out, in distilled water using an ultrasonic bath. This process was performed on the sample M-I and also four times on the sample M-II. The conductivity of

the fluid phase is measured to determine the presence of NaCl in the solid phase and then determining the level of chlorides. After the sample were heated to evaporate for 4 h at 80 °C.

(3) Thermal processing: The products were cooled to room temperature and finally calcined at 425 °C for 4 h. Reddish powder was finally obtained.

As-prepared powder samples M-I and M-II, were characterized X-ray powder diffractometer (XRD). The XRD used was Philips PW1710 BASED X-Ray Diffractometer with 2θ values range, from 10° to 89.98^o and Cu Kα radiation source (λ = 1.54274) operating at 38 kV and 23 mA. The morphology of sample M−II was characterized by scanning electron microscopy (SEM) JEOL JSM-7600F, at a work distance of 5.6 mm. Raman spectra of sample M−II were recorded on a Raman Almega XR (System micro / macro Raman dispersive Nicolet). Infrared spectra of samples M-II were recorded on a Infrared Spectrometer, FTIR Thermo Nicolet NEXUS 670 using KBr matrix.

3. Results and Discussion

Based on a potentiometric titration curve reported in the literature [17], with it the equivalence point system located in a pH of 6.17, by the calculations of the first and second derivatives, was a determined curve. In this curve were identified four regions. In the first region (pH 1.18 to 1.81) occurs a large consumption of OH- ions by the ferric chloride solution (pH 1.18). In the second (pH 1.81 and 2.12), consumption of OH- ions is even greater, since the pH is almost unchanged. Production lots of complex ionic, colliding with each other, clumps together and create larger clusters, called embryos [18]. In the third from (pH 2.12 to 11.91) decreases the speed of embryonic growth, low consumption of OH- ions and increasing pH. This region characterized for nucleation (stable set of embryos) and contains the equivalence point, at which the pH achieves its maximum precipitation [18]. The fourth (pH 11.91 to 13.22) again there is considerable consumption of OH- ions and the dissolution that occurs, slowly reaches saturation. Nuclei are grouped and form hydrated gel [18] ferric oxides. This was taken into account and the synthesis was carried out at pH = 6. The diffractogram Figure 1-(a) y 1-(b) exhibits peaks corresponding to NaCl (PDF pattern 001-1053) [17], peaks are practically absent in the diffraction patterns of powders washed three times; in fact, this assertion is also supported by the conductivity analysis´ aqueous phase resulting from the washings. After the first wash, the conductivity corresponds to 63, 72 mS, value higher than the conductivity of the distilled water (4 μS) [19]. Following the second wash, the con-

ductivity 17, 78 mS. It is 72, 1 % less NaCl from the first washing, and after the third wash 1,32 mS was achieved. Three successive washes caused a 98% salt decline relative to its initial concentration. A certain amount of ions are absorbed in the final product [20]. For this reason, and after removing 98% of the initial products, it was decided to perform only three washes.

X-Ray diffractometer (XRD) was used to identify the crystalline phases. Figure 1-(a) shows the XRD pattern of the sample after heat treatment. The sample shows very thin peaks, indicating the fine nature and small crystallite size of the particles. The result agrees with a $\gamma \rightarrow \alpha\text{-}Fe_2O_3$ phase transformation, that took place during calcination at 450 °C and the weak peaks observed at d-values of 3.68 (D_{012}), 2.69 (D_{104}), 2.51 (D_{110}), 2.19 (D_{113}), 1.84 (D_{024}), 1.69 (D_{116}), 1.59(D_{018}), 1.48 (D_{214}), 1.45 (D_{300}) and 1.30 (D_{1010})Å (peaks marked as 'H'), correspond to (major phase rhombohedral structure) moderate crystalline of $\alpha\text{-}Fe_2O_3$ was identified using the Match Software and literature [21]. Along with peaks at d values of 4.837 (D_{111}), 2.959 (D_{202}), 2.531 (D_{311}), 2.423 (D_{222}), 2.101 (D_{400}), 1.714 (D_{422}), 1.612 (D_{511}) and 1.487 (D_{440}) Å, (minor phase, cubic, and spinel structure) correspond to the $\gamma\text{-}Fe_2O_3$ particles (peaks marked as 'M') and have a cubic unit cells with both octahedrally and tetrahedrally coordinated Fe^{3+} sites (defect spinel structure) [22]. Figure 1-(b) shows the XRD pattern of M−II sample consisted of well crystalline $\gamma\text{-}Fe_2O_3$ (minor phase, cubic, and spinel structure) and $\alpha\text{-}Fe_2O_3$ (major phase) solids with a progressively subsequent increase, in the peak height related to all phases produced, indicating the promotion effect of reaction time in the crystallization degree enhancement of $\alpha\text{-}Fe_2O_3$ and $\gamma\text{-}Fe_2O_3$.
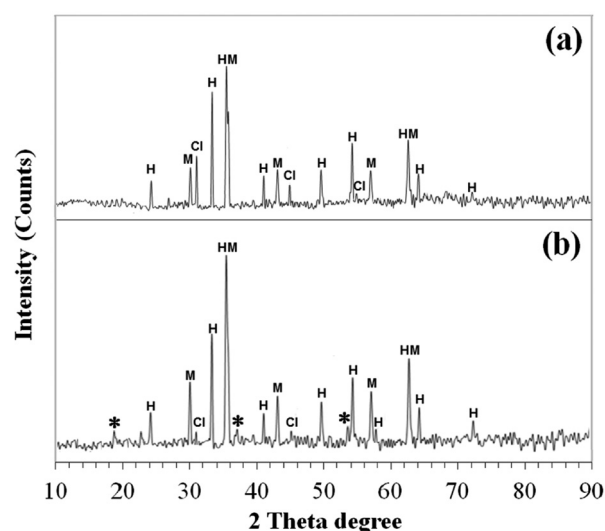

Figure 1. XRD pattern of iron oxide nanoparticles prepared by wet synthesis (a) Sample (M−I) after the first wash, (b) Sample (M−II) after three successive washes (**H** = $\alpha\text{-}Fe_2O_3$, **M** = $\gamma\text{-}Fe_2O_3$, ***** = Fe_3O_4 and **Cl** = Halide).

Due to new peaks 18.38° (D_{111}), 30.20° (D_{220}) and 53.90° (D_{422}) in the diffraction pattern of the sample M-II Figure 4- (b), one cannot overlook the presence of Fe_3O_4 phase depending on the similarity between the diffraction lines, both phases of γ-Fe_2O_3 and Fe_3O_4. From X-ray analysis, the lattice constant so obtained for alpha-Fe_2O_3 nanoparticles were a=b=5.0380 Å and c=13.7720 Å. The lattice parameter "a" and interplanar spacing D_{hkl} γ-Fe_2O_3 (a = 8.3000 Å and D_{311}=2.531 Å), were determined by Bragg's [23] and these values are closed to the values in some references as in (a=8.347 Å and D_{311}=2.517 Å) [24]. The values which are obtained for the sample, can be attributed to simultaneous formation of another phase such Fe_3O_4 (a=8.3958 Å and D_{311}=2.531 Å) [25]. Thus we can conclude that the M−I and M−II samples consisted of moderate crystalline α-Fe_2O_3 and γ-Fe_2O_3 phases, only whereas the M-II sample contain a mixture of α-Fe_2O_3, γ-Fe_2O_3 and Fe_3O_4 phases. A peak width in 2.51 (D_{110}) Figure 1-(b) is increased as the reaction time becomes longer and can be explained by the phase transformations and the effect of washing process, generating more crystallites. This is an interesting observation because sheetlike magnetite impurities, were not reported in the synthesis of hematite by the controlled precipitation method.

The α-crystallites obtained showed sizes below 100 nm similar to that of γ−crystallite. However, the peak height of the diffraction lines at d-spacing 2.69 (D_{104}) and 2.51 (D_{110}) were considered respectively as a α-Fe_2O_3 and γ-Fe_2O_3 phases crystallinity degree measure. It is clear that the increase in reaction time and repeated washings brought about an increase in the different phases crystallinity degree. A progressive shift of all diffraction peaks to higher Bragg angle was observed. This shift displays the presence of changes in both the crystallinity and crystallite size of the investigated solids. The enhancement effects of reaction time and repeated washings on the phase transformation process, are better investigated by measuring the height of certain diffraction lines characteristic for α-Fe_2O_3 (D_{104}), (0.269 nm, 100%) and relative to one of the common lines of both α-Fe_2O_3 (D110), (0.251, 75%) and γ-Fe_2O_3 (0.251, 100%). This was done and the results obtained revealed that the ratio, R, between the peak height of the lines at "d" spacing of 0.251 and 0.269 nm for the M-I sample was 1.53 and was twice the value of R for the pure sample α-Fe_2O_3 (0.75), indicating the formation of γ-Fe_2O_3 phase, due to a partial conversion of some α-Fe_2O_3 to γ-Fe_2O_3 phase. The increasing reaction time in the investigated solids from 24 to 48 hours, led to 1.17, an 25 % growth in the R value, which then decreases, but it is still greater than the pure α-Fe_2O_3 phase one. These observations indicate that the M-I y M-II samples may contain the amorphous γ-Fe_2O_3 phase and nanocrystalline α-Fe_2O_3 phase [26].

Surface morphology of the as-synthesis and calcined samples was studied using SEM analysis. Some samples were observed using metallographic microscope (results not shown). Figure 2 shows the SEM images of the as-prepared Fe_2O_3 nanoparticles by controlled precipitation method. In this figure closest and smaller approach, the particles prepared with formation of clusters or aggregates of particles. In both cases, the aggregates are formed of primary particles whose dimensions can be said that are in the order of nanometers according to the scale of photograph. This indicates that Hematite nanoparticles can be obtained with 24-48 hours of reaction and 425 ºC. When the picture closest approach is achieved, Figure 2(a), you can see that the aggregates are formed by hemispherical and nearly elongated primary particles whose size, apparently, is on the order of nanometers Figure 2(b).
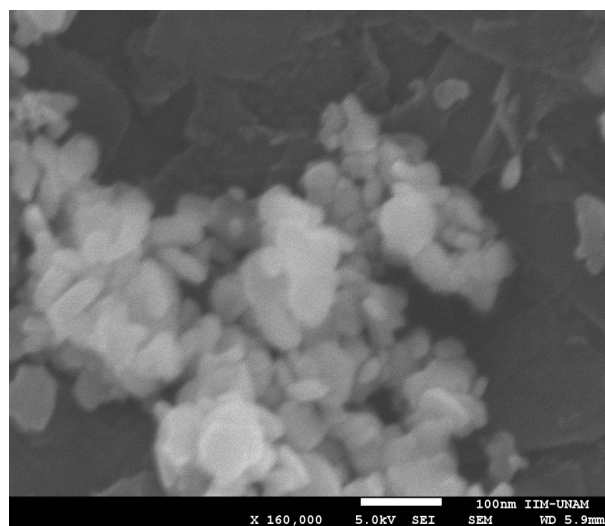
(a)
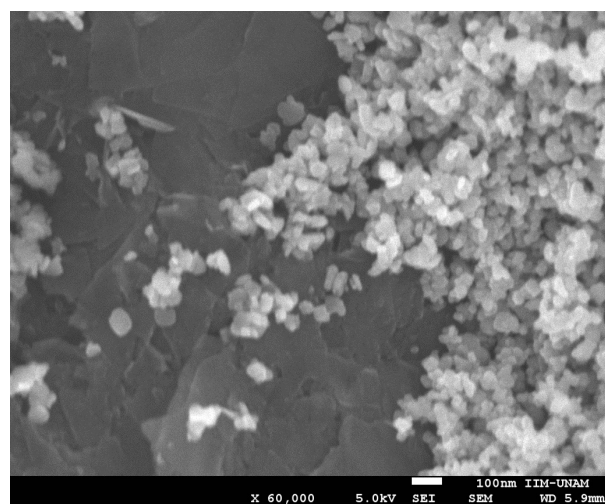
(b)

Figure 2. SEM image of hematite nanoparticles α-Fe_2O_3. Sample (M−II) after three successive washes (a) Closest approach Figure and (b) Smaller approach.

According to Figure 3, the infrared spectrum (FTIR) of the synthesized Fe_2O_3 nanoparticles, was in the range of 400 - 4000 cm^{-1} wavenumber which identifies the chemical bonds, as well as functional groups in the compound. The peaks at 1612.6 cm^{-1} and 3442.8 cm^{-1} can be attributed to the stretching vibration of the hydroxyl groups, on the surface of the nanoparticles, [21] possibly as a contamination of the sample at the time of taking the spectrum or distortions in the signals, probably due to ambient water molecules intrusion [39]. The characteristic absorption sample bands at 549,8 and 457,6 cm^{-1}, may correspond to Fe-O stretching and bending vibration mode of α-Fe_2O_3 respectively [27]. However they are very close at two broad peaks at 555 and 463 cm^{-1} which corresponds to the Fe-O stretching and bending vibration mode, respectively of γ-Fe_2O_3 [28].
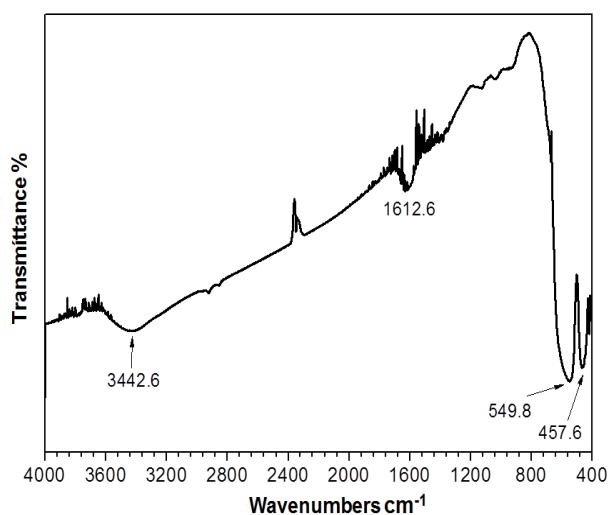

Figure 3. FTIR spectrum of Fe_2O_3 sample. Sample (M-II) after three successive washes
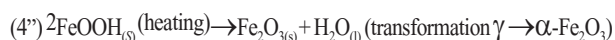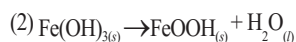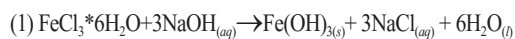
Raman spectroscopy can provide clear assignment of the iron oxide polymorphs through the observation of the phonon modes. The iron oxides species exhibit distinct Raman signatures; therefore, it is possible to take advantage of the so-called phonon confinement effects, to confirm the oxide present in the sample [29]. In order to demonstrate accurately the type of oxide present in the system, a Raman spectrum of nano-powder is presented in Figure 4. Hematite belongs to the D^6_{3d} crystal space group and seven phonon lines are expected in the Raman spectrum [30]. Five of the seven Raman active bands of hematite, that are predicted by group theory, were observed with the different intensities: Namely a A_{1g} mode (493.8 cm^{-1}) and three E_g modes (299.7, 399.8 and 607.6 cm^{-1}). The most representative bands of hematite are around 228.6 cm^{-1} and 295.02 cm^{-1} [31], however only one was found in our spectrum (299.7 cm^{-1}). From the literature, the band at about 1305.7 cm^{-1}, is a vibration which has some unclear origin. Faria *et al.* [31] says that this band is caused

by the scattering of two magnons in the structure, but according to Su *et al.* [32], this phonon consists of a second harmonic vibration.

It is important to say that the band of hematite at 1305.7 cm^{-1}, is close to the magnetite at approximately 1304.9 cm^{-1}. This causes an overlapping in vibrations when these two phases are mixed, making difficult their identification by using those bands. In the case of magnetite, the most representative band is found at about 653.6 cm^{-1}. The results make it possible to distinguish hematite from magnetite (Fe_3O_4) characterized by a specific band at 661.6 cm^{-1} [32]. In the Raman spectrum, the bands between 600 and 700 cm^{-1}, which appear both in the experimental spectrum and the theoretical, differ because the relative intensities thereof are reversed. This behavior indicates the possible presence of $\gamma \rightarrow \alpha$-$Fe_2O_3$ and Fe_3O_4 different phases in the sample. Furthermore, in the experimental spectrum band nearby 200 cm^{-1} does not appear, which is in line with the previous behavior.

At a relatively high hydrogen-ion activity and high electron activity (an acidic reducing medium), iron (II) ion, Fe^{2+}, is the predominant iron species. At a very high hydrogen-ion activity and low electron activity (an acidic oxidizing medium) Fe^{3+} ion predominates. In an oxidizing medium at lower acidity, solid $Fe(OH)_3$ is the primary iron species present. Finally, in a basic reducing medium, with low hydrogen-ion activity and high electron activity, solid $Fe(OH)_2$ can be stable. Within the pH regions normally (approximately pH 5-9) $Fe(OH)_3$ or Fe^{2+} is the predominant stable iron species. In fact, it is observed that in medium containing dissolved oxygen at any appreciable level (a relatively high pE), hydrated iron (III) oxide $Fe(OH)_3$ is essentially the only inorganic iron species found. Medium contain a high of suspended iron, but any truly soluble iron must be in the complex form. In highly anoxic low-pE medium, appreciable levels of Fe^{2+} may be present. However when such medium is exposed to atmospheric oxygen, the pF rises and $Fe(OH)_3$ precipitates [33].

The precipitation is obtained when the amount of $FeCl_3.6H_2O$ and NaOH solution reaches a stoichiometric condition. At the equivalence point, the iron ions in the solution have a positive charge of +2, and therefore the synthesis starts from ferrous ions by reacting with hydroxyl ions, produce iron oxide (III) Hydrated [17], and the following reactions are proposed for the mechanism of the nanopowders synthesized here [34-37]:

(1) $FeCl_3 * 6H_2O + 3NaOH_{(aq)} \rightarrow Fe(OH)_{3(s)} + 3NaCl_{(aq)} + 6H_2O_{(l)}$

(2) $Fe(OH)_{3(s)} \rightarrow FeOOH_{(s)} + H_2O_{(l)}$

(3') $2FeOOH_{(s)} + Fe^{2+}_{(aq)} + 2OH^-_{(aq)} \rightarrow Fe_3O_{4(s)} + 2H_2O_{(l)}$

(4") $2FeOOH_{(s)}$ (heating) $\rightarrow Fe_2O_{3(s)} + H_2O_{(l)}$ (transformation $\gamma \rightarrow \alpha$-$Fe_2O_3$)

From Eq. (1), (2) and (3'), it is suggested that the precipitation obtained in the first step of nanoparticle synthesis is FeOOH, or goethite [34] and the ferric and ferrous hydroxides are precipitated. These reactions are very fast. Second, the ferric hydroxide decomposes to FeOOH Ec. (2), due to the low water activity of the resulting NaCl solution in a slower reaction. Finally, a solid state reaction between FeOOH and $Fe(OH)_2$ takes place Ec (3'), due to the low water activity of the solution. Ferrous hydroxide $(Fe(OH)_2)$ formed from the reaction of Fe^{2+} and hydroxyl ion, could not be consumed rapidly because the solid phase reaction progressed relatively slowly [38]. This was supported by the fact that much of the FeOOH still remained even after 24-48 h, as shown in Figure 4(a) and 4(b). The overall reaction mechanism is a dynamic equilibrium equation in which the concentration and size of Fe_3O_4 nanoparticles are influenced by $[Fe^{3+}]$, $[Fe^{2+}]$ and $[OH^-]$, as well as the water activity of the solution. [35].

The crystal growth mechanism might be the combination of O-R and O-A pathways. It can explain the increase of particle size of the obtained nanoparticles with increasing the reaction time, greater number of washes (comparison of DRX sample M-I and M-II, Figure 1(a) and 1(b)). It is obtained when it was stirred for 48 hours at room temperature and washed three times. This is due a higher chance for crystal growth to take place in the process. To
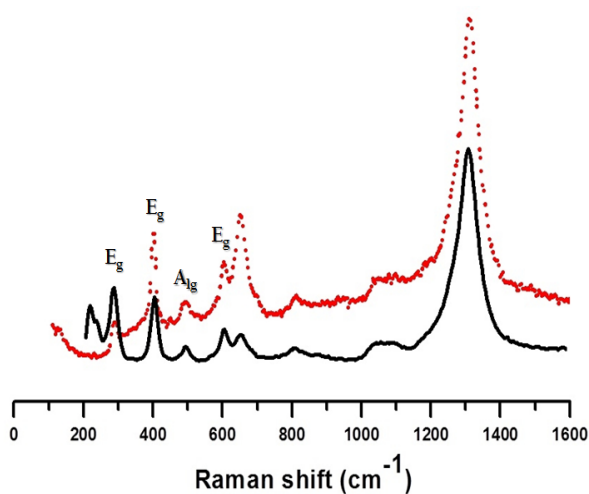

Figure 4. Raman spectrum of hematite (••••) experimental, (--) theoretical [17]

a lesser extent, Fe(II) concentration and stirring of the suspension, also influence the nature of the final product, but mainly affect the kinetics of the reaction. Important variations of these parameters led to the formation of other phases.

The last step is the calcination process Ec. (3"). A secondary stage of crystal growth happens in this step. It can explain the effect of temperature calcination in the hematite nanoparticles formation. The calcined process was an incomplete crystal growth process. There are two well-known crystalline types of Fe_2O_3: maghemite (the γ-phase) with cubic structure and hematite (the α-phase) with rhombohedral structure. The phase transition of $\gamma \rightarrow \alpha$-$Fe_2O_3$ takes place during calcination at about 450 °C [36]. The phase transformation which occurs during calcination, gives rise to transform α-Fe_2O_3 powder which has undergone considerable aggregation and grain growth [37]. The characteristics of the obtained hematite nanoparticles were influenced by the parameters in every step of the sample preparation that is a mixing process, increasing the reaction time, greater number of washes and stirring, plus calcination processes.

4. Conclusion

A simple controlled precipitation synthesis has been successfully carried out to fabricate α-Fe_2O_3 nanopowders at a relatively low temperature. The synthesis method of Fe_2O_3 nano-particles was investigated with a focus on the structural and surface morphological properties, the relationship synthesis-structure and the nature of Fe_2O_3 nano-crystallites. It was clarified that the reaction time repeated washings and convective force used in the synthesis process, played an important role in determining the transformation of the iron oxides and particle size and phase. Formation/transformation of phases at different reaction time and repeated washings was confirmed by XRD analysis. This is an interesting observation because magnetite impurities were not reported in the synthesis of hematite by the controlled precipitation method. From SEM (scanning electron microscopy) images, exhibits the synthesized Fe_2O_3 nanopowders by controlled precipitation route with an average diameter < 100 nm and the morphology of the aggregates particles, is from plate-like shaped nearly hemispherical and elongated, due that nanometric primary particles are spheroidal form and have a possibly join to form small linear agglomerates, and structures that can be "transformed" into tablets, rods or bars. FTIR data, showed the presence of Fe-O stretching mode of Fe_2O_3. With the help of the Raman spectra, the

nanopowders were clearly identified, mainly as hematite mixed with maghemite by their spectral bands and the lattice parameter "a" and inter-planar spacing D_{hkl} characteristic. Magnetite impurities removal by simple oxidation can generate a mixture of hematia and maghemite nanopowders with potential application. This mixture of metal oxides nanoparticles could be of great importance for the removal of toxic heavy metals from subsurface, technological and Industrial applications.

Acknowledgment

References

[1]   L. Huo, W. Li, L. Lu, H. Cui, S. Xi, J. Wang, B. Zhao, Y. Shen, and Z. Lu, "Preparation, structure, and properties of three-dimensional ordered α-Fe2O3 nano-particulate film", *Chem. Mater.*, vol. 12, no. 3, pp. 790, 2000.

[2]   R.H. Kodama, S.A. Makholoufand, and A.E. Berkowitz, "Finite size effects in antiferromagnetic NiO nanoparticles", *Phys. Rev. Lett.*, vol. 79, no. 7, pp. 1393-1396, 1997.

[3]   W.T. Dong, and C.S. Zhu, "Use of ethylene oxide in the sol–gel synthesis of α-Fe2O3 nanoparticles from Fe(III) salts", *J. Mater. Chem.*, vol. 12, no. 6, pp. 1676, 2002.

[4]   A. Prakash, A.V. McCormick, and M.R. Zachariah, "Aero-Sol-Gel synthesis of nanoporous iron-oxide particles: A potential oxidizer for nanoenergetic materials", *Chem. Mater.*, vol. 16, no. 8, pp. 1466-1471, 2004.

[5]   A.K. Gupta, and M. Gupta, "Synthesis and surface engineering of iron oxide nanoparticles for biomedical applications", *Biomaterials,* vol. 26, no. 18, pp. 3995-4021, 2005.

[6]   A. Figuerola, R.D. Corato, L. Manna, and T. Pellegrino, "From iron oxide nanoparticles towards advanced iron-based inorganic materials designed for biomedical applications", *Pharmacological Research,* vol. 62, no. 2, pp. 126-143, 2010.

[7]   M. J. Espín, A.V. Delgado, J. E. Martin, "Effects of electric fields and volume fraction on the rheology of hematite/silicone oil suspensions", *Rheol Acta,* vol. 44, pp. 71-79, 2004.

[8]   L. Huo, Q. Li, H. Zhao, L. Yu, S. Gao, J. Zhao, "Sol-gel route to pseudocubic shaped α-Fe$_2$O$_3$ alcohol sensor: Preparation and characterization", *Sensors Act. B: Chem*, vol. 107, pp. 915-920, 2005.

[9]   S. Pandey, S. Misha, "Sol-gel derived organic-inorganic hybrid materials: Synthesis, characterizations and applications", *J. Sol-Gel Sci. Technol.*, vol. 59, pp. 73-94, 2011.

[10] Q. Wenqing, Y. Congren, Y. Ran, and G. Guanhua, "Hydrothermal Synthesis and Characterization of Single-Crystalline α-Fe$_2$O$_3$ Nanocubes", *J. Nanomat*, 2011, pp. 1-5, 2011.

[11] A. Burukhin, B. Churagulov, N. Oleynikov, V. Knot'ko, "Hydrothermal synthesis of mesoporous iron oxide powders", *Joint Sixth International Symposium on Hydrothermal Reactions and Fourth Conference on Solvo-Thermal Reactions*, Kochi, Japan, pp. 561-564. 25-28 July, 2000.

[12] K. Byrappa, T. Adschiri, "Hydrothermal technology for nanotechnology", *Prog. Cryst. Grow. Ch. Mat.*, vol. 53, pp. 117-166, 2007.

[13] S. Park, H. Kheel, G. Sun, T. Ko, W. In Lee, and Ch. Lee1, "Acetone Gas Sensing Properties of a Multiple-Networked Fe$_2$O$_3$-Functionalized CuO Nanorod Sensor", *J. Nanomat,* 2015, pp. 1-5, 2015.

[14] L. Diamandescu, D. Mihaila-Tarabasanu, N. Popescu-Pogrion, "Hydrothermal transformation of α-FeOOH into α-Fe$_2$O$_3$, in the presence of silicon oxide", *Mater Lett,* vol. 27, pp. 253-25, 1996.

[15] H. Karami, "Synthesis and Characterization of Iron Oxide Nanoparticles by Solid State Chemical Reaction Method", *J. Cluster Sci.*, vol. 21, pp. 11-20, 2010.

[16] J. Rockenberger, E.C. Scher, A.P. Alivisatos, "A New Nonhydrolytic Single-Precursor Approach to Surfactant-Capped Nanocrystals of Transition Metal Oxides", *J. Am. Chem. Soc.*, vol. 121, pp. 11595-11596, 1999.

[17] M. de los Á Berrones, L. Lascano, "Síntesis de nanopartículas de hematita por el método de precipitación controlada", *Revista Politécnica*, vol. 30, pp. 91-99, 2009.

[18] J. Rodríguez, "Síntesis de polvos cerámicos por el método de precipitación", *Boletín de la Sociedad Española de Cerámica y Vidrio*, vol. 40, pp. 173-184, 2001.

[19] R. Perry, D. Green, J. Maloney, *Manual del Ingeniero Químico*, 7ma ed., Madrid: McGraw Hill, 2001.

[20] U. Schwertmann and R. Cornell, *Iron Oxides in the Laboratory - Preparation and Characterization*, 2da Ed., Weinheim, Germany: John Wiley and Sons Ltd., 2000.

[21] (a) M. Farahmandjou and F. Soflaee, "Synthesis and Characterization of α-Fe$_2$O$_3$ Nanoparticles by Simple Co-Precipitation Method", *Phys. Chem. Res.*, vol. 3, no. 3, pp. 191-196, 2015. (b) K. Petcharoena, A. Sirivat, "Synthesis and characterization of magnetite nanoparticles via the chemical co-precipitation method", *Mater Sci and Eng B*, vol. 177, pp. 421-427, 2012.

[22] S.K. Sahoo, K. Agarwal, A.K. Singh, B.G. Polke and K.C. Raha, "Characterization of γ- and α-Fe$_2$O$_3$ nano powders synthesized by emulsion precipitation-calcination route and rheological behaviour of α-Fe$_2$O$_3$", *Int. J. Eng. Sci. Technol,* vol. 2, pp. 118-126, 2010.

[23] B.D. Cullity, S.R. Stock, *Elements of X-ray Diffraction*, New Jersey, 2001.

[24] L. Victoria, D del C. Calero, C. Rinald, "Synthesis and magnetic characterization of cobalt-substituted ferrite(Co$_x$Fe$_{3-x}$O$_4$) nanoparticles", *J. Mag. Mag. Mat.,* vol. 314, pp. 60-67, 2007.

[25] V. Kumar, A. Rana, M.S. Yadav, R.P. Pant, "Size-induced effect on nano-crystalline CoFe$_2$O$_4$", *J. Mag. Mag. Mat*. 320, 1729-1734, 2008.

[26] N.M. Deraz, A. Alarifi, "Novel processing and magnetic properties of hematite/maghemite nano-particles", *Ceramics Int.,* vol. 38, pp. 4049-4055, 2012.

[27] B. Zhao, Y. Wang, H. Guo, J. Wang, Y. He, Z. Jiao, M. Wu, "Iron oxide (III) nanoparticles fabricated by electron beam irradiation method", *Materials Science Poland,* vol. 25, no. 4, pp. 1143-1148, 2007.

[28] T. Kim Il, G. A. Nunnery, K. Jacob, J. Schwartz, X. Liu, and R. Tannenbaum, "Synthesis, characterization, and alignment of magnetic carbon nanotubes tethered with maghemite nanoparticles", *J. Phys. Chem. C,* vol. 114, no. 15, pp. 6944-6951, 2010.

[29] A. M. Jubb and H. C. Allen, "Vibrational spectroscopic characterization of hematite, maghemite, and magnetite thin films produced by vapor deposition", *ACS Applied Materials and Interfaces*, vol. 2, no. 10, pp. 2804-2812, 2010.

[30] N. Buzgar, A. I. Apopei, A. Buzatu, Romanian Database of Raman Spectroscopy (online), available at http://rdrs.uaic.ro/contact.html.

[31] D.L.A. de Faria, S. Venancio Silva, M.T. de Oliveira, "Raman microscopy of some iron oxides and oxyhydroxides", *J. Raman Spectrosc.*, vol. 28, pp. 873-878, 1997.

[32] X. Su, C. Yu, C. Qiang, "Synthesis of α-Fe$_2$O$_3$ nanobelts and nanoflakes by thermal oxidation and study to their magnetic properties, *Appl. Surf. Sci.*, vol. 257, 9014-9018, 2011.

[33] S. E. Manahan, Water Chemistry – Green Science and Technology of Nature´s Most Renowable Resourse, CRC Press, E.U.A, pp 102-103, 2011.

[34] T. Nurhayati, F. Iskandar, M. Abdullah and Khairurrijal, "Syntheses of Hematite (α-Fe$_2$O$_3$) Nanoparticles Using Microwave-Assisted Calcination Method", *Mater. Sci. Forum*, vol. 737, pp 197-203, 2013.

[35] M. C. Mascolo, Y. Pei and T. A. Ring, "Room Temperature Co-Precipitation Synthesis of Magnetite Nanoparticles in a Large pH Window with Different Bases", *Mater.*, vol. 6, pp. 5549-5567, 2013.

[36] B. Wang, Q. Wei, Sh. Qu, "Synthesis and Characterization of Uniform and Crystalline Magnetite Nanoparticles via Oxidation-precipitation and Modified co-precipitation Methods", *Int. J. Electrochem. Sci*., vol. 8, pp. 3786-3793, 2013.

[37] J. Morales, J.L. Tirado, C. Valera, "Preferential X-ray line broadening and thermal behavior of γ-Fe$_2$O$_3$", *J. Am. Ceram. Soc.*, vol. 72, pp. 1244-1246, 1989.

[38] T. Iwasaki, N. Sato, H. Nakamura, S. Watano, "An experimental investigation of aqueous-phase synthesis of magnetite nanoparticles via mechano-chemical reduction of goethite", *Adv Powder Tech*, vol. 24, pp. 482-486, 2013.

[39] J. M. Chalmers, "Mid-infrared spectroscopy; Anomalies, Artifacts and Common Errors in Using Vibrational Spectroscopy Techniques in Handbook of Vibrational Spectroscopy", in J.M. Chalmers and P.R. Griffiths (eds.), Chichester: Jhon Wile and Sons Ltd., pp. 2327-2347, 2002.